DETECTION AND RECOGNITION OF LUNG NODULES IN SPIRAL CT IMAGES USING DEFORMABLE TEMPLATES AND BAYESIAN POST-CLASSIFICATION

Aly Farag[1], *Ayman El-Baz*[1], *G.Gimel'farb*[2], *and Robert Falk*[3]

[1]CVIP Laboratory
University of Louisville
Louisville, KY, USA
{farag,elbaz}@cvip.uofl.edu

[2]CITR, Tamaki Campus
University of Auckland
Auckland, New Zealand
g.gimelfarb@aukland.ac.nz

[3]Director, Medical Imaging Division
Jewish Hospital
Louisville, KY, USA
robert.falk@jhhs.org

ABSTRACT

In this paper, we propose a novel algorithm for isolating lung abnormalities (nodules) from low dose spiral chest CT scans. The proposed algorithm consists of three main steps. The first step isolates the lung nodules, arteries, veins, bronchi, and bronchioles from the surrounding anatomical structures. The second step detects lung nodules using deformable 2D and 3D templates describing typical geometry and gray level distribution within the nodules of the same type. The detection combines the normalized cross-correlation template matching and genetic optimization algorithm. The final step eliminates the false positive nodules (FPNs) using three features that robustly define the true lung nodules. Accurate density estimation for these three features is obtained using logistic regression model and linear combination of Gaussians (LCG) with positive and negative components. This paper focuses on the second and third steps. Experiments with 200 patients' CT scans demonstrate the accuracy of our approach.

1. INTRODUCTION

Lung cancer is one of the most common and lethal types of cancer. In 1999, there were approximately 170,000 new cases of lung cancer [3]. Early detection of lung tumors (visible on chest film as nodules) may increase the patients chance of survival. But detecting nodules is a complicated task; see, e.g., [4]. Nodules show up as relatively low-contrast white circular objects within the lung fields. The difficulty for CAD schemes is to distinguish true nodules from arteries, veins, and ribs.

At present, low-dose spiral computer tomography (LDCT) is of prime interest for screening public groups of high risk to early detect lung cancer [3]. The LDCT provides chest scans with very high spatial, temporal, and contrast resolution of anatomic structures and is able to gather a complete 3D volume of human thorax in a single breath hold [4]. The automatic screening typically involves two-stage detection of lung abnormalities (nodules). First, the initial candidate nodules are selected, and then the false candidates called false positive nodules (FPNs) are partially eliminated while preserving the true ones (TPNs).

At the first stage, conformal nodule filtering [5] or unsharp masking [6] can enhance nodules and suppress other structures as to separate the candidates from background by simple thresholding. To improve the separation, background trend is corrected in [7] within image regions of interest. Circular nodule candidates can be detected by usual template matching [6] or Hough transform [8].

The FPNs are excluded at the second stage by feature extraction and classification [7, 9]. Such features as circularity, size, contrast [7], or local curvature [9] are extracted by morphological techniques, and artificial neural networks (ANN) are frequently used as post-classifiers [10]. The critical issue is to adequately discriminate between the nodules and non-nodules.

In this paper nodule types are modelled with the four central-symmetric deformable templates such as (*i*) solid spheric model of large-size (above 12 mm) calcified and non-calcified nodules appearing in several successive slices, (*ii*) hollow spheric model of large lung cavity nodules, (*iii*) circular model of small nodules appearing in only a single slice, and (*iv*) semicircular model of lung wall nodules. This approach allows for isolating abnormalities which spread over several adjacent CT slices.

Each template has a specific gray level pattern which is analytically estimated in order to fit the available empirical data. The normalized cross-correlation is used for the template matching. The 3D or 2D position, size, and gray level pattern of each template is adjusted to the most similar part of the segmented veins, arteries, and lung abnormalities by genetic optimization technique [11]. After all the candidates are detected, a supervised Bayesian classification of geometric and textural features of the candidate nodules excludes partially the FPNs.

0-7803-8554-3/04/$20.00

2. DEFORMABLE TEMPLATES OF ABNORMALITIES

Our detection of lung nodules begins with two segmentation stages which considerably reduce the search space. At the first stage shown in Figs. 1(a) and 1(b), the lungs are separated from surrounding anatomical structures, e.g., ribs, liver, and other organs, appearing in the chest CT scans. The second stage extracts arteries, veins, bronchi, and lung abnormalities (see Fig. 1(c)) from the already segmented lungs. Segmentation algorithms are based on representing each CT slice as a sample of a Markov–Gibbs random field of region labels and gray levels. Details of the algorithms are presented in [1, 2]. Figure 1(d) shows the empirical

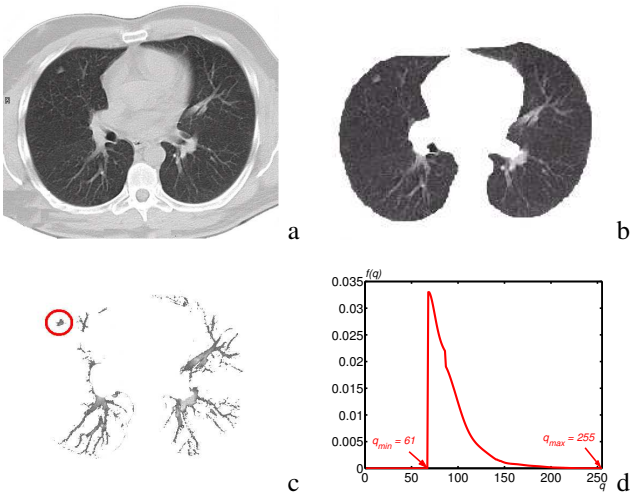

Fig. 1. First two segmentation steps.

gray level distribution over the extracted regions in Fig. 1(c). Because both the nodules and normal tissues such as arteries, veins, and bronchi, have almost the same gray level distributions, the abnormality detection should involve their geometrical features, too. Four basic classes of the lung abnormalities are small calcified, large calcified, non-calcified, and cavity nodules. The first three classes tend to solid spherical shapes, whereas the cavity nodules are hollow spheres. Generally, the smaller nodules appear only in a single 2D slice whereas the larger ones spread over a 3D volume represented by several successive slices. Lung wall nodules may also appear in one or more slices, depending on their size. However, they are semicircular in shape.

Our analysis of 2D CT slices suggests that spatial changes of gray levels across the central cross-section of a solid-shape 3D nodule or across a solid-shape 2D one can be approximated with a central-symmetric Gaussian-like template $q(r) = q_{\max} \exp\left(-(r/\rho)^2\right)$; $0 \le r \le R$. Here, r and $q(r)$ are the radius from the template's center to and the gray level in a template point with Cartesian coordinates (ξ, η) with respect to the center (i.e., $r^2 = \xi^2 + \eta^2$), $q_{\max}$ denotes the maximum gray level for the template, R is the template radius depending on the minimum gray level $q_{\min} = q(R)$, and the parameter ρ specifies how fast the signals decrease across the template.

3. TEMPLATE IDENTIFICATION AND MATCHING

The CT slices in our study have spatial resolution of 0.4 mm per pixel so that the radius range for all lung nodules is $R = 5$–30 pixels. Because the third spatial axis has lower resolution, for large solid and hollow lung nodules we use the 3-layer template. Thin lung nodules appearing only in a single slice have the circular templates. The lung wall nodules are of semicircular shape. We assume that the template deformations other than translations are restricted to different scales (radii) of all the templates and also different orientation angles of the semicircular ones. Examples of the deformed templates are presented in Fig. 2.

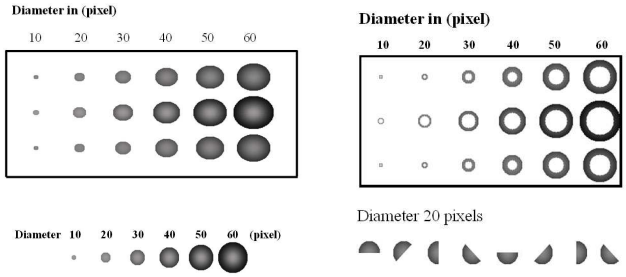

Fig. 2. Templates of solid and hollow 3D large nodules, 2D small nodules, and semicircular lung wall nodules.

The gray level distribution density over the 2D Gaussian-like template is easily found in the closed form:

$$\psi(q|q_{\min}, q_{\max}) = 2\pi R \sqrt{\frac{lnq_{max} - lnq}{lnq_{max} - lnq_{min}}} \qquad (1)$$

This relationship allows us to roughly estimate the template parameters $q_{\max}$ and $q_{\min}$ from the empirical density in Fig. 1(d) (in this particular case $q_{\max} = 255$ and $q_{\min} = 61$). The parameter ρ relates to the template radius R as follows: $\rho = R\left(\ln q_{\max} - \ln q_{\min}\right)^{-\frac{1}{2}}$. In particular, for the circular templates of the radii $R = 5$ and 30 the estimated $\rho = 4.18$ and 25.08, respectively. Figure 3 demonstrates how close is the empirical gray level distribution for the objects in Fig. 1(c) to the estimated distribution for the above two templates under its discretization.

In the case of the 3D solid spherical templates, the 2D template is first identified for the central cross-section. Then the upper and lower cross-sections are specified by using the same parameters in the following equation ($q_t(r) = q_{\max} \exp\left(-\left(r^2 + t^2\right)/\rho^2\right)$) where t is the slice thickness

in pixels ($t = 7$ in our experiments below). The radius of upper and lower circles is specified by the relationship $q_t(R) = q_{\min}$.

The hollow spherical templates to detect cavity lung nodules are obtained in a similar way by removing the central part of the solid templates up to 75% of the radius R.

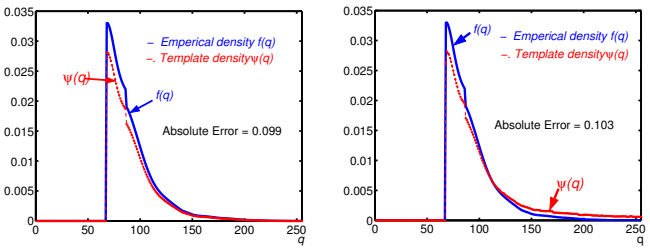

$R = 5$ $R = 30$

Fig. 3. Estimated template gray level distributions ($\psi(q)$) w.r.t. the empirical density ($f(q)$).

We use the normalized cross-correlation as the similarity measure. The search for the template's position, size, and angle (for the semicircular template) maximizing the correlation in a given 3D image is performed by genetic optimization [11]. The latter has 9-, 6-, 5-, and 7-bit resolution for the (x, y)-coordinates in the CT slices, z-coordinate across the stack of the slices, template radius R, and angle of the semicircular template, respectively. The matching algorithm runs separately for each type of the lung abnormalities, and all spatial locations where the similarity score is greater than a certain threshold (in our experiments 0.8) are extracted as the candidate nodules.

4. POST-CLASSIFICATION OF NODULE FEATURES

Because actual lung nodules are not exactly spherical, circular, or semicircular, some true nodules can be missed as well as a number of false positive nodules (FPNs) can be encountered during the initial extraction of the candidates. To reduce the error rate, the post-classification of the candidate nodules is performed with the following three textural and geometric features of each detected nodule: (*i*) radial non-uniformity $U = \max_{\theta}(d(\theta)) - \min_{\theta}(d(\theta))$ of its borders (here, $d(\theta)$ is the distance at the angle θ between the center of the template and the border of the segmented object as shown in Fig. 4(d)); (*ii*) mean gray level (q_{ave}) over the 3D or 2D nodular template; and (*iii*) the 10%-tile gray level for the marginal gray level distribution over the 3D or 2D nodular template. To distinguish between the FPNs and TPNs, we use a supervised Bayesian classifier on a training set of false and true nodules. The three features (*i*)–(*iii*) are used to classify the FPNs in the lungs, while only the last two features are applied to the lung wall nodules. The density estimation required in the Bayes classifier is performed, for each feature, using logistic regression model and linear combination of Gaussians (LCG) with positive and negative components.

4.1. Density Estimation using Logistic Regression Model and LCG

Logistic regression is a member of the family of generalized linear models. It has found extensive applications in biological, biomedical and environmental problems [12]. In this section we show how to use logistic regression model to get accurate density that represent each feature.

The estimated density $p(y)$ using the logistic regression model is given by

$$p(y) = \frac{\beta_1 e^{\beta_1 y}}{(1 + e^{-(\beta_0 + \beta_1 y)})^2} + \varepsilon \qquad (2)$$

where $\beta_0 + \beta_1 y$ is called the linear predictor, y represents the realized value of the current feature, and ε is the error term. In this paper we assume that the three features are independent, hence the estimation for the density for each feature is done separately.

From Eq. (2) we need to estimate three parameters in order to calculate $p(y)$. These three parameters are β_0, β_1, and ε. β_0 and β_1 are estimated by minimizing the square distance between the empirical density $f(y)$ and estimated density $p(y)$ using simplex method. Table 1 shows the estimated parameters for both FPNs and TPNs for the three features.

Because the empirical density for each feature does not follow exactly the logistic model, there will be deviation between the empirical density and the estimated density. This deviation is represented in the error term ε, which can be modelled by linear combination of Gaussian (LCG) with positive and negative components. The number of positive and negative components and the estimated parameters for each component is obtained using modified EM algorithm proposed in [2]. Figure 4 shows the empirical and estimated density for each feature for both TPNs and FPNs.

Table 1. Estimated parameters for logistic regression model for each feature for both TPNs and FPNs.

Parameters	Radial non-uniformity		Mean gray level		10%-tile gray level	
	TNs	FPNs	TNs	FPNs	TNs	FPNs
β_0	-3.7	-3.8	-13.7	-19.2	-9.4	-24.4
β_1	0.9	0.2	0.1	0.1	0.1	0.2

5. EXPERIMENTAL RESULTS AND CONCLUSIONS

The algorithm was tested on the CT scans of 200 subjects. Among these scans, twenty one show abnormalities, and the rest were normal. At stage 1, the template matching extracted 110 true candidates (out of the true 130 nodules) and 49 FPNs. The classification at the stage 2 reduced the

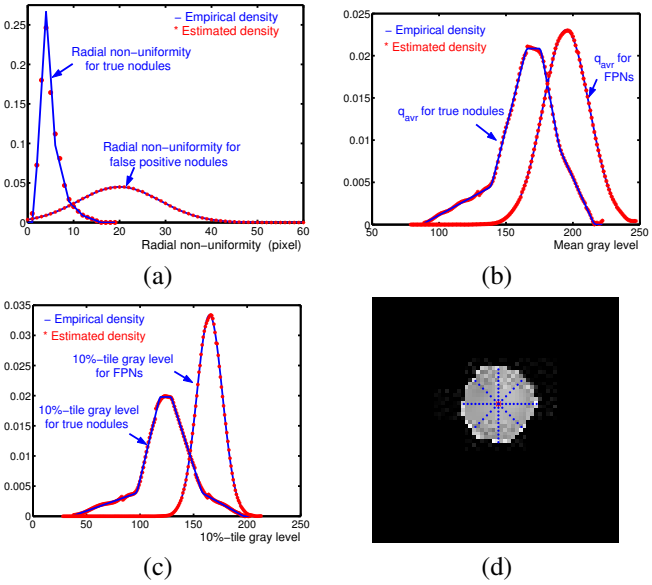

Fig. 4. (a) $f(y)$ and $p(y)$ for radial non-uniformity, (b) $f(y)$ and $p(y)$ for mean gray level, (c) $f(y)$ and $p(y)$ for 10%-tile gray level, and (d) shows the calculation of $d(\theta)$ at 8 direction

number of the FPNs to 12 but simultaneously rejected three true nodules. Thus the final number of the TPNs became 107 out of 130 giving the overall correct detection rate of 82.3% with the FPNs rate of 9.2%. Table 2 presents the numbers of TPNs and FPNs before ($TPNs_1$; $FPNs_1$) and after ($TPNs_2$; $FPNs_2$) the post-classification stage. Our

Table 2. Detection rate for different types of abnormalities (TPNs : the nodules determined by a radiologist).

Nodule type	$TPNs_1$	$FPNs_1$	$TPNs_2$	$FPNs_2$
Lung wall	28 : 29	8	27 : 29	2
Calcified	46 : 49	4	46 : 49	1
Non-calcified	12 : 18	5	12 : 18	3
Cavity	8 : 11	7	8 : 11	1
Small	17 : 23	25	15 : 23	5

experiments show that the proposed adaptive deformable templates, with straight forward analytical parameter estimation, allow for detecting more than 80% of the true lung abnormalities. The number of the simultaneously detected false nodules can be considerably reduced by accounting for simple geometrical and textural features of the candidate nodules. But it is still difficult to accurately detect small lung nodules similar to bronchi and bronchioles. Our future work includes the selection of features that distinguish between small lung nodules and normal objects.

Acknowledgement *This research has been supported by grants from the Jewish Hospital Foundation and the Kentucky Lung Cancer Program.*

6. REFERENCES

[1] A. A. Farag, A. El-Baz, and G.L.Gimel'farb, "Precise Image Segmentation by Iterative EM-Based Approxiation of Empirical Grey Level Distributions with Linear Combinations of Gaussions", in *IEEE Workshop on Learning in Computer Vision and Pattern Recognition*, Washington, DC, USA, July, 2004.

[2] G.L.Gimel'farb, A. A. Farag, and A. El-Baz, "ExpectationMaximization for a Linear Combination of Gaussians", in *Proc. IEEE Int. Conf. on Pattern Recognition (ICPR 2004)*, Cambridge, United Kingdom, August, 2004.

[3] P. M. Boiselle and C. S. White (Eds.) *New Techniques in Thoracic Imaging*. M. Dekker, New York, 2002.

[4] L. Quekel, A.Kessels, R. Goei, and J. V. Engelshoven, "Miss rate of lung cancer on the chest radiograph in clinical practice," *Chest*, Vol. 115, no. 3, pp. 720–724, 1999.

[5] S.-C. B. Lo, M. T. Freedman, J.-S. Lin, and S. K. Mun, "Automatic lung nodule detection using profile matching and back-propagation neural network techniques," *J. Digital Imaging*, Vol. 6, no. 1, pp. 48–54, 1993.

[6] F. Mao, W. Qian, J. Gaviria, and L. Clarke, "Fragmentary window filtering for multiscale lung nodule detection," *Academic Radiology*, Vol. 5, no. 4, pp. 306–311, 1998.

[7] X. Xu, S. Katsuragawa, K. Ashizawa,H. MacMahon, and K. Doi, "Analysis of image features of histograms of edge gradient for false positive reduction in lung nodule detection in chest radiographs," *Proc. SPIE*, Vol. 3338, pp. 318–326, 1998.

[8] W. Lampeter, "ANDS-V1 computer detection of lung nodules," *Proc. SPIE*, Vol. 555, pp. 253–261, 1985.

[9] M. J. Carreira, D. Cabello, M. G. Penedo,and J. M. Pardo, "Computer aided lung nodule detection in chest radiography," in R. T. Chin et al. (Eds.) *Image Analysis Applications and Computer Graphics*, (*Lecture Notes in Computer Science* 1024), Springer, Berlin, pp. 331–338, 1995.

[10] J. S. Lin, S. B. Lo, A. Hasegawa, M. T. Freedman, and S. K. Mun, "Reduction of false positives in lung nodule detection using a two-level neural classification," *IEEE Trans. Med. Imaging*, Vol. 15, pp. 206–216, April 1996.

[11] D. E. Goldberg, *Genetic Algorithms in Search, Optimization and Machine Learning*. Addison-Wesley, Reading, Mass., 1989.

[12] R. H. Myers, D. C. Montgomery, and G. G. Vining, *Generalized Linear Models*, John Wiley & Sons, Inc., New York, 2002.